

# Chiral Majorana hinge modes on a curved surface with magnetic impurities

Ilyoun Na,<sup>1,2,3,\*</sup> James G. McHugh,<sup>4,5</sup> Sinéad M. Griffin,<sup>2,3</sup> and Luca Chiroli<sup>1,6</sup>

<sup>1</sup>*Department of Physics, University of California, Berkeley, California 94720, USA*

<sup>2</sup>*Materials Sciences Division, Lawrence Berkeley National Laboratory, Berkeley, California 94720, USA*

<sup>3</sup>*Molecular Foundry, Lawrence Berkeley National Laboratory, Berkeley, CA 94720, USA*

<sup>4</sup>*University of Manchester, School of Physics and Astronomy, Manchester M13 9PL, United Kingdom*

<sup>5</sup>*National Graphene Institute, University of Manchester, Manchester M13 9PL, United Kingdom*

<sup>6</sup>*NEST, Scuola Normale Superiore, and Istituto Nanoscienze-CNR, I-56127 Pisa*

(Dated: October 16, 2023)

Chiral Majorana one-dimensional modes have been proposed as they key component for topological quantum computing. In this study, we explore their potential realization as hinge modes in higher-order topological superconductors. To create such phases, we engineer a sign-changing, time-reversal symmetry-breaking mass term through an ensemble of magnetic impurities on the surface of a sphere. The magnetization of this ensemble arises from the competition between the external magnetic field and the Ruderman-Kittel-Kasuya-Yosida (RKKY) interaction among the impurities, mediated by the surface Majorana modes. We determine the magnetic phase diagram and identify the optimal magnetic field to minimize orbital effects and induce a sign changing mass term. This term opens a gap in the surface spectrum, resulting in a gapless one-dimensional chiral Majorana mode along the nodal line of the mass term, thereby implementing a second-order topological superconductor.

*Introduction.*—Chiral Majorana one-dimensional (1D) modes are much sought after for their potential application in topological quantum computing [1–7] – topological superconductors (TSCs) [8–12] offer a promising platform for isolating these modes. In tandem with the search for these modes, remarkable progress has been made in higher-order topology [13–21], which extends the conventional first-order bulk-boundary correspondence, providing more possible avenues for realizing Majorana modes.

In this letter, we present a method for creating higher-order TSCs by introducing symmetry-breaking perturbations to gap out the one-dimensional lower boundary modes of first-order topological phases. For instance, applying a Zeeman field in a two-dimensional (2D) time-reversal invariant (TRI) TSC results in Majorana corner states [22]. Extending this approach to the surface of a three-dimensional (3D) TRI TSC with a magnetic field generates chiral Majorana hinge modes along lines tangent to the surface [23, 24]. However, challenges arise in 3D superconductors due to the presence of Meissner screening, which leads to the emergence of an orbital supercurrent. This supercurrent couples with surface Majorana modes, tilting the surface spectrum and becoming dominant over the Zeeman term as the applied field strength increases [25, 26].

To address this, we propose decorating the surface of a 3D TRI TSC with magnetic impurities. The net Zeeman field is given by the sum of the external field and the magnetic moments of the impurities. Aligning the magnetic impurities with the direction of the field locally enhances the Zeeman term without affecting the orbital supercurrent, thus increasing the strength of the nodal time-reversal symmetry-breaking mass term. However, a potential obstacle to this proposal is the self-ordering of the magnetic impurities through the Ruderman-Kittel-

Kasuya-Yosida (RKKY) interaction. Similar to the case of a topological insulator (TI) [27], coupling magnetic impurities with surface Majorana modes in a planar geometry results in a ferromagnetic RKKY interaction due to the Ising properties of Majorana surface fermions [28], leading to magnetic order.

We generalize the Ising properties of Majorana surface fermions and the resulting RKKY interaction, demonstrating its role in promoting a ferromagnetic radial order that competes with the external magnetic field. In the absence of an applied field, impurities form a hedgehog configuration resembling a magnetic monopole. With a sufficiently strong field, the ground state undergoes a phase transition to a domain wall state. We illustrate that the critical field for the onset of the domain wall state decreases as the number of impurities increases. Consequently, in systems with dense enough magnetic impurity ensembles, the resulting mass term opens a gap in the surface spectrum, leaving a gapless chiral Majorana mode along the nodal line at the equator.

*Second-order TSC with Zeeman field.*—We illustrate the realization of a chiral Majorana mode along the inversion-symmetric line, which is protected by intrinsic higher-order bulk topology [17, 29]. To create a second-order TSC, we start with the massless surface (flat) states of a first-order 3D TRI odd-parity class DIII TSC [24, 30, 31]. By adding a sign-changing mass term  $V(y) = \text{sgn}(y)V_z$  to the surface Hamiltonian, which is represented as  $H = -iv(\partial_x\sigma_y - \partial_y\sigma_x) + V(y)\sigma_z$  with Pauli matrices  $\sigma_i$  denoting the spin degree of freedom, we generate a chiral mode propagating in the  $x$  direction and localized at mass term node. This mass term can be effectively regarded as a Zeeman term due to its interaction with the spin degree of freedom. In a spherical geometry, we introduce the sign changing mass term

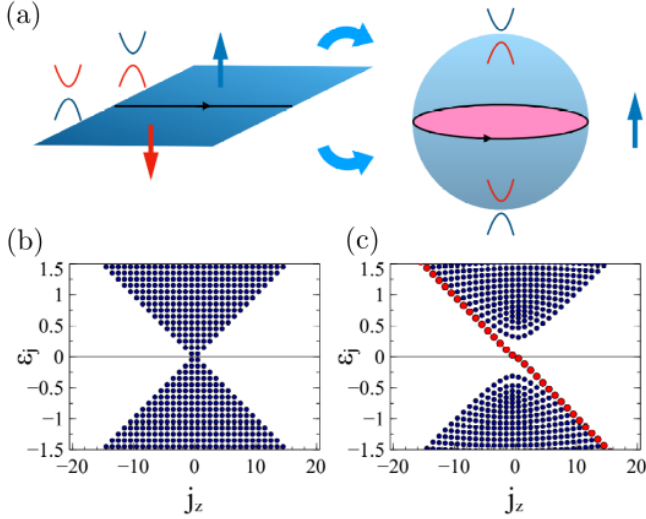


FIG. 1. (a) Schematic illustration of how second-order TSC can be realized along the inversion-symmetric curve on the surface of a sphere using a uniform Zeeman field along the polar axis preserving the inversion symmetry. (b) The surface energy spectrum of the Dirac Hamiltonian on the surface of sphere defined in Eq. (1) without, and (c) with a Zeeman field.

by applying a uniform Zeeman field along the polar axis, breaking the time-reversal symmetry while preserving inversion symmetry. This setup results in the emergence of a single chiral Majorana mode along the inversion-symmetric equator, where the mass term vanishes, as illustrated in Fig. 1(a). This realization represents a second-order TSC of class D with inversion symmetry, topologically classified by  $\mathbb{Z}_2$  [29].

*Chiral Majorana hinge modes on sphere.*—We introduce gamma matrices  $\gamma^i \equiv (\gamma^0, \gamma^1, \gamma^2) = (-i\sigma_z, \sigma_x, \sigma_y)$  in flat 2+1-dimensional Minkowski space with  $\{\gamma_i, \gamma_j\} = 2\eta_{ij}$  and  $\eta_{ij} = \text{diag}(-1, 1, 1)$ . In curved space-time, the  $\eta_{ij}$  is now replaced the metric tensor  $g_{\mu\nu}$ , giving new gamma matrices  $\gamma^\mu$  satisfying  $\{\gamma^\mu, \gamma^\nu\} = 2g^{\mu\nu}$ . The resulting Dirac equation in curved space-time takes the form  $\hbar v_\Delta \gamma^0 [-i\gamma^\mu(x) D_\mu] \psi = 0$  [32, 33]. Here, the covariant derivative  $D_\mu = \partial_\mu + \Gamma_\mu$  results, with the spin connection  $\Gamma_\mu$  originating from local Lorentz transformations.

On the surface of a sphere with radius  $R$ , the metric is given by  $g_{\mu\nu} = \text{diag}(-1, R^2, R^2 \sin^2 \theta)$ . This results in the gamma matrices [34],  $\gamma^0 = -i\sigma_z$ ,  $\gamma^1(x) = \gamma^1/R = \sigma_x/R$ , and  $\gamma^2(x) = \gamma^2/R \sin \theta = \sigma_y/R \sin \theta$ . The spin connection is  $\Gamma_\mu = -\frac{1}{2} \sigma_z \cos \theta \delta_{2\mu}$ . Consequently, the Dirac Hamiltonian on the surface of the sphere is given by [25, 35–37],

$$h_0^{cur} = \frac{\Delta}{k_F R} \gamma^0 \left[ -i\sigma_x \left( \partial_\theta + \frac{\cot \theta}{2} \right) - i \frac{\sigma_y}{\sin \theta} \partial_\phi \right]. \quad (1)$$

The eigenstates of Eq. (1) can be represented using Jacobi polynomials  $|\Upsilon_{lm}^\sigma\rangle$ , where  $l$  denotes the angular mo-

mentum,  $m$  is the projection along the polar axis, and  $\sigma = \pm 1$  is the particle-hole index. The corresponding eigenenergies are given by  $\epsilon = \text{sgn}(\sigma)(l + 1/2) \frac{\Delta}{k_F R}$ , with  $l$  taking half-integer values [36, 38–40]. For each  $l$ , there are  $2l + 1$  degenerate states, as shown in Fig. 1(b). The presence of the spin connection induces a gap in the surface energy spectrum of the Majorana Dirac cone, which scales proportionally to  $1/R$ .

We now introduce a Zeeman term into the Hamiltonian in Eq. (1). The Ising properties of surface Majorana modes [28] in a planar geometry only allow the orthogonal spin component  $s_\perp$  to the plane to be a relevant perturbation.  $s_\perp$  is mapped to  $\sigma_z$  in the Majorana representation, and thus, the Zeeman term  $\mathbf{V} \cdot \mathbf{s}$  can be written as  $h_Z = V_\perp \sigma_z$ . The normal to the local tangential plane at any given point on the surface of a sphere corresponds to the radial component. Then, the uniform Zeeman field  $\mathbf{V}$  applied in the axial direction generates the mass term as  $V_\perp = V \cos \theta$ . In accordance with inversion symmetry requirements, the mass term  $V(\mathbf{r}) = \mathbf{V}_\perp$  satisfies  $V(\mathbf{r}) = -V(-\mathbf{r})$  from  $V \cos \theta = -V \cos(\theta + \pi)$ . The mass term vanishes along the equator at  $\theta = \pi/2$ , where the Zeeman field is tangential to the surface.

The Zeeman term has two consequences. First, it generates finite matrix elements between positive and negative energy states of the Hamiltonian in Eq. (1), leading to an additional gap in the spectrum. These matrix elements are given by

$$\begin{aligned} \langle \Upsilon_{lm}^+ | \sigma_z \cos \theta | \Upsilon_{l'm'}^- \rangle &= i \delta_{mm'} \frac{\sqrt{(l+1)^2 - m^2}}{2(l+1)} \delta_{l', l+1} \quad (2) \\ &- i \delta_{mm'} \frac{\sqrt{l^2 - m^2}}{2l} \delta_{l', l-1}. \end{aligned}$$

Additionally, the perturbation results in non-trivial diagonal matrix elements [3],

$$\langle \Upsilon_{lm}^\pm | \sigma_z \cos \theta | \Upsilon_{l'm'}^\pm \rangle = \delta_{m, m'} \delta_{l, l'} \frac{m}{2l(l+1)}. \quad (3)$$

These matrix elements induce non-trivial results. They cause an upward energy shift in all states with positive  $m$ , which is particularly pronounced in low-energy states with small  $l$ . Conversely, they induce a downward energy shift in all states with negative  $m$ . For states with  $l = |m|$ , the energy shift undoes the gapping, resulting in a single chiral mode crossing the gap, as shown in Fig. 1(c).

*RKKY interaction among magnetic impurities on a sphere.*—As largely discussed in [3], applying an external Zeeman field comes at the price of an orbital tilting effect on Bogoliubov deGennes (BdG) and surface Majorana spectra that dominates over the Zeeman term upon increasing the field. To address this issue and enable the realization of Majorana modes with reduced field strength and enhanced insensitivity to this tilting effect, we introduce magnetic impurities on the surface. These impurities, denoted as  $\mathbf{S}_i$  and positioned at locations  $\mathbf{R}_i$ ,

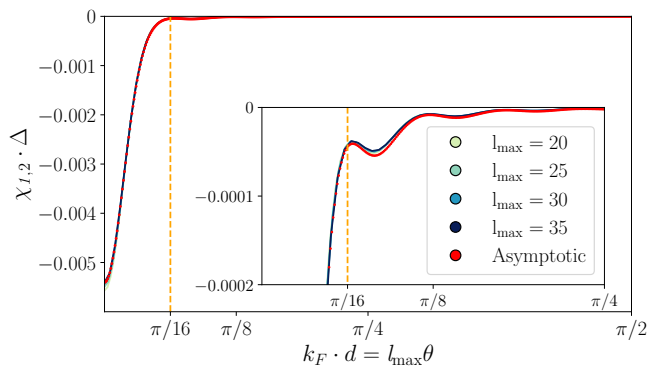


FIG. 2. The dimensionless static susceptibility  $\chi_{1,2} \cdot \Delta$  as a function of the dimensionless distance  $k_F \cdot d = k_F \cdot R\theta = l_{\max}\theta$ , where  $l_{\max} = k_F R$  represents the upper limit for the summation over  $l$  in Eq. (6), and  $\theta$  denotes the angle between neighboring impurities on the sphere with radius  $R$ . The negative sign of the RKKY coupling coefficient,  $J^R = \lambda^2 \chi_{1,2}$ , implies a ferromagnetic Ising RKKY interaction among the radial components of impurities. We obtain its asymptotic form in Eq. (7), which serves as a valid approximation based on the plot.

interact with the surface Majorana modes. For simplicity, we use semiclassical descriptions of magnetic impurities and focus exclusively on the on-site exchange interaction between these impurities and the surface Majorana modes. Due to the locality, the exchange term on a curved surface involves only the radial component of the magnetic moment  $S_i^r$  at its location, taking the form as

$$h_{\text{ex}}^{\text{cur}} = i\gamma_0 \lambda \sum_i S_i^r \delta(\mathbf{x} - \mathbf{R}_i) \frac{1}{\sqrt{|g|}}, \quad (4)$$

with the interaction strength  $\lambda$ . Here,  $g$  represents the determinant of the metric  $g_{\mu\nu}$ , and it can be eliminated through an appropriate rescaling of the wavefunction,  $\Psi \rightarrow \chi = |g|^{1/4} \Psi$ .

The magnetic impurities experience RKKY interactions mediated by propagating surface Majorana modes. We can evaluate the RKKY interaction on the curved surface by integrating out the Majorana modes and expanding with their Green's function up to second order in  $\lambda$ . The resulting expression is

$$H^{\text{RKKY}} = \lambda^2 \sum_{i,j} \chi_{ij} S_i^r S_j^r, \quad (5)$$

where  $\chi_{ij} \equiv \chi(\mathbf{R}_i, \mathbf{R}_j) = -\langle T s_1^r(\mathbf{R}_1, \tau) s_2^r(\mathbf{R}_2, 0) \rangle$  represents the out-of-plane spin susceptibility of the surface modes, with  $\tau$  denoting imaginary time. Its one loop approximation is given by  $\chi_{i,j}(i\nu_n) = -1/\beta \sum_{i\nu_n} \text{Tr}[s_i^r \hat{G}_0(\mathbf{R}_i, \mathbf{R}_j, i\nu_n + i\omega_n) s_j^r \hat{G}_0(\mathbf{R}_j, \mathbf{R}_i, i\omega_n)]$ . Here,  $\beta = 1/T$  ( $k_B \equiv 1$ ) and  $\omega_n = 2\pi/\beta \cdot (n + 1/2)$  represents the Matsubara frequency [41]. In this expression,  $\hat{G}_0 = (i\omega - \hat{h}_0^{\text{cur}})^{-1}$ , and we take a partial trace over

the particle-hole degree of freedom of eigenstates  $|\Psi_{l_m}^\pm\rangle$  of  $\hat{G}_0$ . We confine our system to the low-temperature limit, where  $T \ll \Delta/k_F R$ , simplifying the static susceptibility in the low-energy regime near the gap as

$$\chi_{ij} = - \sum_{l_m, l'_m} \frac{Z_{l_m; l'_m}(\mathbf{R}_j) Z_{l_m; l'_m}^*(\mathbf{R}_i)}{\mathcal{E}_l + \mathcal{E}_{l'}}, \quad (6)$$

where  $Z_{l_m; l'_m}(\mathbf{R}) = \Psi_{l_m}^+(\mathbf{R}) \sigma_3 \Psi_{l'_m}^-(\mathbf{R})$  involving transitions between negative and positive energy states with  $\mathcal{E}_l = (l + 1/2)\Delta/k_F R$ , mediated by the exchange interaction. The sum over  $|m| \leq l < l_{\max} \simeq k_F R$  is bounded below the gap of the bulk energy spectrum, that is an order of  $\Delta$ . We compute the dimensionless static susceptibility  $\chi_{1,2} \cdot \Delta$  as a function of the dimensionless distance  $k_F \cdot d = k_F \cdot R\theta$ , where  $\theta$  is the angle between neighboring impurities. Using the azimuthal symmetry, we simplify the calculation by fixing one impurity at the north pole and placing the other at a latitude  $\theta$  of radius  $R$ . As shown in Fig. 2, a ferromagnetic Ising RKKY interaction emerges among the radial components of impurities, as indicated by the negative sign of  $J^R = \lambda^2 \chi$ .

To characterize the asymptotic behavior of the susceptibility, we calculate it as a function of azimuthal angle  $\phi$  while fixing two impurities along the equator line, allowing us to derive a valid asymptotic form for large values of  $l_{\max}$  and  $\phi \ll \pi$

$$\chi(\phi) = - \frac{k_F}{4\pi^2 R^3 \Delta} \sum_{l, l'=1/2}^{l_{\max}} \frac{(l + 1/2)(l' + 1/2)}{l + l' + 1} \mathcal{F}_{l, l'}(\phi), \quad (7)$$

where  $\mathcal{F}_{l, l'}(\phi) = [J_0(l\phi)J_0(l'\phi) + J_1(l\phi)J_1(l'\phi)]$ . Our comparison with the exact case in Fig. 2 confirms its validity for  $l_{\max} > 20$ . This asymptotic approximation shows a range bounded from above by  $1/R^3$ , similar to the flat surface case [42].

*Magnetic phase diagram.*—With the form and the range of RKKY interaction now established, our focus turns to the magnetic phase diagram. The magnetic moment of the  $i$ -th impurity, denoted as  $\mathbf{S}_i$ , can be parameterized using polar and azimuthal angles,  $\Theta_i$  and  $\Phi_i$ . These angles define the orientation of  $\mathbf{S}_i$  relative to local coordinates  $z_i$  and  $x_i$  in a tangential plane centered at its position  $\mathbf{R}_i = (\theta_i, \phi_i)$ . The free energy of the system is given as a sum of the RKKY interaction and the Zeeman term. Its dependence on  $\Phi_i$  is solely due to the RKKY interaction, and we can set  $\Phi_i = \phi_i$  as a solution of the Euler-Lagrange equations with respect to  $\Phi_i$ , which minimizes the energy functional. Consequently, we are left with

$$H = \sum_{ij} J_{ij}^R \cos(\Theta_i) \cos(\Theta_j) - B \sum_j \cos(\Theta_j + \theta_j), \quad (8)$$

where the  $J_{ij}^R = \lambda^2 \chi_{ij}$ . In a simplified representation of the RKKY interaction, illustrated in Fig. 2, when we confine its spatial influence to nearest neighbor (NN) pairs

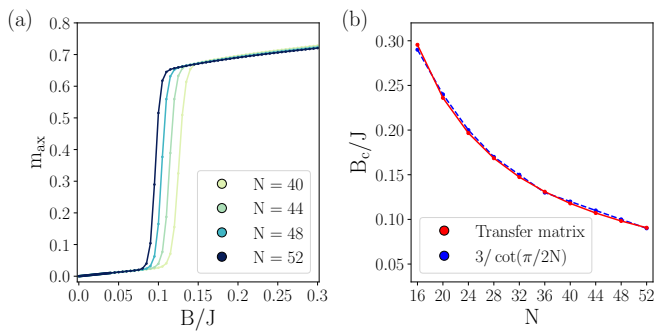


FIG. 3. (a) The magnetization of a system with  $N$  magnetic impurities on the circular geometry, influenced by the RKKY interaction and the external Zeeman field along the axial direction, is computed using the transfer matrix method for the given energy functional  $H$  in Eq. (8). We perform this calculation with  $M = 100$  and set the temperature to  $T/J = 0.1$ . (b) The critical field is represented as a function of  $N$  consistent with the analytic prediction of the phase transition scale from the hedgehog to the domain wall configuration.

by setting  $\chi_{ij} = \chi$  for such pairs  $(i, j)$ . The ferromagnetic Ising RKKY interaction compels the magnetic impurities to arrange themselves radially, forming a hedgehog configuration, with  $\Theta_i$  taking on values of either 0 or  $\pi$ . In contrast, the Zeeman term dictates that impurities align with the external field, adopting an axial configuration with  $\Theta_i = -\theta_i$ . The ground state is determined by the interplay between these two competing terms.

It is instructive to begin by examining the one-dimensional (1D) problem on a circle as a geodesic curve along the sphere. Assuming a uniform distribution of  $N$  impurities with positions set at  $\theta_i = 2\pi i/N$ , we can express the RKKY interaction as  $\chi_N = \chi[\cos(2\pi/N)]$ . The energy for both hedgehog and axial configurations can be written as follows  $E_{\text{hed}} = -N\lambda^2\chi_N$  and  $E_{\text{ax}} = -N\cos(2\pi/N)\lambda^2\chi_N/2 - NB$ .

In the hedgehog configuration, the Zeeman term contributions cancel out due to the exact cancellation of impurities placed at antipodal points. In contrast, the energy in the axial configuration results from both Zeeman term and RKKY interactions. The critical field obtained by equating the energies of the hedgehog and axial configurations, is given by  $B_c/J = 1 - \cos(2\pi/N)/2$ , and it saturates at  $1/2$  for large  $N$ . When considering the energy in a domain wall kink located near the equator, at the intersection of two hemicycles with opposite signs of the local magnetic moment in the radial component, it can be expressed as  $E_{\text{dw}} = -(N-4)\lambda^2\chi_N - B\cot(\pi/2N)$ .

For the domain wall configuration to become the ground state, the Zeeman term must dominate over the RKKY interaction along the domain wall, that is for  $\cot(\pi/2N) > 4\lambda^2\chi_N/B$ . By neglecting the  $N$  dependence of  $\chi_N$  for large  $N$  and defining the RKKY interaction strength as  $J = \lambda^2\chi$ , the critical field for the phase transition from zero total magnetization to

finite magnetization along the axial direction scales as  $B_c/J = 4/\cot(\pi/2N)$ , revealing an inverse relationship between increasing  $N$  and decreasing critical field.

To validate the results obtained from the approximate analytic estimate, we calculate the magnetization and study its behavior with an increasing number of magnetic impurities  $N$ . The partition function at temperature  $T$  is given by  $Z = \int \prod_i^N \frac{d\Theta_i}{2\pi} \exp[-H\{\{\Theta_i\}\}/T] \equiv \exp[-F/T]$ , where  $F$  represents the free energy. We discretize the magnetic configurations of  $i$ -th impurity as  $\Theta_i = 2\pi n_i/M$  for a sufficiently large  $M$ , and employ the transfer matrix method to compute the partition function. The magnetization along the axial direction is determined as  $m_{\text{ax}} = -\frac{1}{N} \frac{\partial F}{\partial B}$ . In Fig. 3(a), we present a plot of the magnetization versus the applied field  $B$  at  $T/J = 0.1$  for different numbers of magnetic impurities. Notably, we observe a non-linear decrease in the critical field as  $N$  increases, following a behavior of approximately  $3/\cot(\pi/2N)$  in close agreement with the analytic prediction for the critical field of the phase transition from the hedgehog to the domain wall configuration, as shown in Fig. 3(b).

The analysis on the 2D surface can be approached similarly. Assuming a uniform distribution of impurities on the sphere, we can do a triangulation of the sphere with  $N$  impurities occupying  $N_v = N$  equally distanced vertices. Here, our aim is not to provide an exact account of each impurity position, but rather to offer a qualitative estimate of the phase diagram and an approximate understanding of how it depends on the number of impurities. For every triangulation, the number of edges  $N_e$  and triangles  $N_t$  are related through  $N_e = 3(N-2)$ ,  $N_t = 2(N-2)$ . On the surface with a radius of  $R$ , each triangle has an area of  $4\pi R^2/N_t = d^2\sqrt{3}/4$ , where  $d = R\theta_d$  represents the average distance between two nearest neighbors, and the neighboring arch angle  $\theta_d$  is given by  $\theta_d = \sqrt{16\pi/(N_t\sqrt{3})} \equiv \theta_g/\sqrt{N}$ . Neglecting the dependence on  $N$  for  $\chi_N = \chi[\cos(\theta_g/\sqrt{N})]$  when  $N$  is large, the energy in a hedgehog configuration is expressed as

$$E_{\text{hed}} = -3(N-2)J, \quad (9)$$

with  $J = \lambda^2\chi_N$ . In the axial configuration, the RKKY contribution to the energy can be estimated by integrating over the Northern hemisphere, given as  $E_{\text{ax}}^{\text{RKKY}} = -(3NJ/2) \int_0^{\pi/2} d\theta \sin\theta \cos^2\theta$ , which considers the projection along the radial direction. This leads to the energy of the axial configuration as

$$E_{\text{ax}} \sim -NJ - NB. \quad (10)$$

In the domain wall configuration, the RKKY contribution is determined by the energy of hedgehog configuration minus twice the energy of the domain wall near the equator. The Zeeman term in the continuum limit

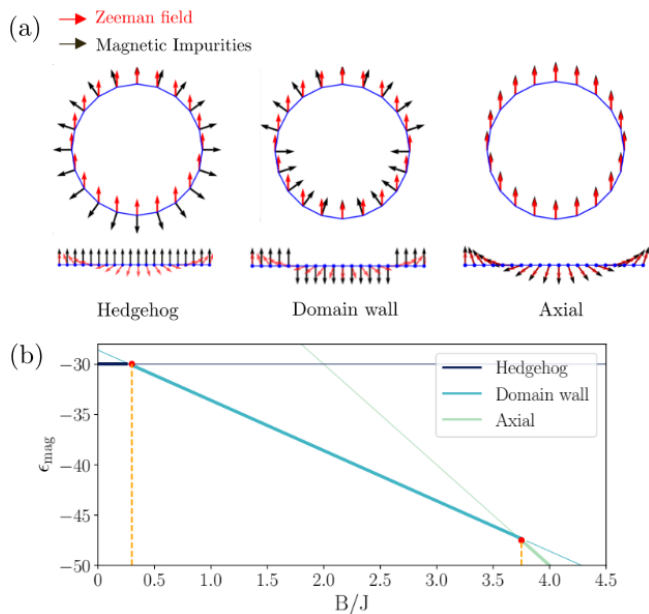


FIG. 4. (a) The magnetic moments of impurities along the geodesic in each configuration. (b) The energy density of a system of  $N = 2000$  impurities on the surface of a sphere subjected to RKKY interaction and an external magnetic field along the axial direction, as described by Eq. (9), (10), and (11).

can be calculated as  $E_{\text{dw}}^Z = -NB/2 \int_0^{\pi/2} d\theta \sin \theta \cos \theta - NB/2 \int_{\pi/2}^{\pi} d\theta \sin \theta \cos(\pi - \theta)$  resulting in the following expression

$$E_{\text{dw}} \sim -(3N - 2\sqrt{10N})J - \frac{NB}{2}, \quad (11)$$

where  $\sqrt{10N}$  represents the number of edges cutting the equator at the intersection of two hemispheres with opposite signs of local magnetic moment in a radial order. As previously discussed in the 1D geodesic case, the ground state can exhibit a domain wall configuration when the Zeeman term surpasses the RKKY interaction along the equator, which occurs for  $B > 4J\sqrt{10/N}$  whereas the critical field scales as  $1/N$  for large  $N$  in the 1D case.

*Conclusion.*—We realize a second-order chiral Majorana hinge mode along the inversion-symmetric equator by modifying a 3D TRI odd-parity TSC. This involves introducing a uniform external Zeeman field to break time-reversal symmetry while preserving inversion symmetry. As the magnetic field increases, the orbital tilting effect on the surface energy spectrum takes precedence over the Zeeman term. To counteract this, we introduce surface magnetic impurities, proposing that the chiral mode emerges in a domain wall configuration with a reduced magnetic field strength. We analyze the ferromagnetic Ising RKKY interaction among the radial components of these impurities, deriving its asymptotic form converging to the interaction form on a flat surface as the radius of sphere increases. We examine scenarios with 1D

and 2D impurities, determining the critical field for the transition to a domain wall configuration hosting a chiral Majorana mode. Detailed investigations of how these obtained chiral hinge modes can be utilized for interferometers [43, 44] is left for future work.

*Acknowledgement.*—This work (I.N, S.M.G.) was supported by the US Department of Energy, Office of Science, National Quantum Information Science Research Centers, Quantum Systems Accelerator (QSA). Computational resources were provided by the National Energy Research Scientific Computing Center and the Molecular Foundry, DOE Office of Science User Facilities supported under Contract No. DEAC02-05-CH11231. This project (L.C.) has received funding from the European Union’s Horizon 2020 research and innovation program under the Marie Skłodowska-Curie Grant Agreement No. 841894 (TOPOCIRCUS). L.C. also acknowledges EU’s Horizon 2020 Research and Innovation Framework Programme under Grant No. 964398 (SUPERGATE) and No. 101057977 (SPECTRUM).

\* ilyoun1214@berkeley.edu

- [1] Chetan Nayak, Steven H. Simon, Ady Stern, Michael Freedman, and Sankar Das Sarma, “Non-abelian anyons and topological quantum computation,” *Rev. Mod. Phys.* **80**, 1083–1159 (2008).
- [2] Sankar Das Sarma, Michael Freedman, and Chetan Nayak, “Majorana zero modes and topological quantum computation,” *npj Quantum Information* **1**, 15001 (2015).
- [3] Luca Chiroli, José Pablo Baltanás, and Diego Frustaglia, “Chiral majorana interference as a source of quantum entanglement,” *Phys. Rev. B* **97**, 155416 (2018).
- [4] Biao Lian, Xiao-Qi Sun, Abolhassan Vaezi, Xiao-Liang Qi, and Shou-Cheng Zhang, “Topological quantum computation based on chiral majorana fermions,” *Proceedings of the National Academy of Sciences* **115**, 10938–10942 (2018).
- [5] Yizhi You, Daniel Litinski, and Felix von Oppen, “Higher-order topological superconductors as generators of quantum codes,” *Phys. Rev. B* **100**, 054513 (2019).
- [6] Raditya Weda Bomantara and Jiangbin Gong, “Measurement-only quantum computation with floquet majorana corner modes,” *Phys. Rev. B* **101**, 085401 (2020).
- [7] Tudor E. Pahomi, Manfred Sigrist, and Alexey A. Soluyanov, “Braiding majorana corner modes in a second-order topological superconductor,” *Phys. Rev. Research* **2**, 032068 (2020).
- [8] A. Yu Kitaev, “Unpaired majorana fermions in quantum wires,” *Physics-Uspekhi* **44**, 131 (2001).
- [9] Xiao-Liang Qi and Shou-Cheng Zhang, “Topological insulators and superconductors,” *Rev. Mod. Phys.* **83**, 1057–1110 (2011).
- [10] Jason Alicea, “New directions in the pursuit of majorana fermions in solid state systems,” *Reports on Progress in Physics* **75**, 076501 (2012).

- [11] Karsten Flensberg, Felix von Oppen, and Ady Stern, “Engineered platforms for topological superconductivity and majorana zero modes,” *Nature Reviews Materials* **6**, 944–958 (2021).
- [12] Sankar Das Sarma, “In search of majorana,” *Nature Physics* **19**, 165–170 (2023).
- [13] Zhida Song, Zhong Fang, and Chen Fang, “ $(d - 2)$ -dimensional edge states of rotation symmetry protected topological states,” *Phys. Rev. Lett.* **119**, 246402 (2017).
- [14] Josias Langbehn, Yang Peng, Luka Trifunovic, Felix von Oppen, and Piet W. Brouwer, “Reflection-symmetric second-order topological insulators and superconductors,” *Phys. Rev. Lett.* **119**, 246401 (2017).
- [15] Wladimir A. Benalcazar, B. Andrei Bernevig, and Taylor L. Hughes, “Quantized electric multipole insulators,” *Science* **357**, 61–66 (2017).
- [16] Frank Schindler, Ashley M. Cook, Maia G. Vergniory, Zhijun Wang, Stuart S. P. Parkin, B. Andrei Bernevig, and Titus Neupert, “Higher-order topological insulators,” *Science Advances* **4**, eaat0346 (2018), <https://www.science.org/doi/pdf/10.1126/sciadv.aat0346>.
- [17] Eslam Khalaf, “Higher-order topological insulators and superconductors protected by inversion symmetry,” *Phys. Rev. B* **97**, 205136 (2018).
- [18] Eslam Khalaf, Hoi Chun Po, Ashvin Vishwanath, and Haruki Watanabe, “Symmetry indicators and anomalous surface states of topological crystalline insulators,” *Phys. Rev. X* **8**, 031070 (2018).
- [19] Yang Peng and Gil Refael, “Floquet second-order topological insulators from nonsymmorphic space-time symmetries,” *Phys. Rev. Lett.* **123**, 016806 (2019).
- [20] Yang Peng, “Floquet higher-order topological insulators and superconductors with space-time symmetries,” *Phys. Rev. Res.* **2**, 013124 (2020).
- [21] Yan-Bin Yang, Jiong-Hao Wang, Kai Li, and Yong Xu, “Higher-order topological phases in crystalline and non-crystalline systems: a review,” (2023), [arXiv:2309.03688](https://arxiv.org/abs/2309.03688) [cond-mat.mes-hall].
- [22] Xiaoyu Zhu, “Tunable majorana corner states in a two-dimensional second-order topological superconductor induced by magnetic fields,” *Phys. Rev. B* **97**, 205134 (2018).
- [23] G. E. Volovik, “Topological superfluid  $^3\text{He-B}$  in magnetic field and ising variable,” *JETP Letters* **91**, 201–205 (2010).
- [24] Liang Fu and Erez Berg, “Odd-parity topological superconductors: Theory and application to  $\text{Cu}_x\text{Bi}_2\text{Se}_3$ ,” *Phys. Rev. Lett.* **105**, 097001 (2010).
- [25] Luca Chirolli and Francisco Guinea, “Magnetic tilting and emergent majorana spin connection in topological superconductors,” *Phys. Rev. B* **98**, 094515 (2018).
- [26] Luca Chirolli and Francisco Guinea, “Signatures of surface majorana modes in the magnetic response of topological superconductors,” *Phys. Rev. B* **99**, 014506 (2019).
- [27] D. A. Abanin and D. A. Pesin, “Ordering of magnetic impurities and tunable electronic properties of topological insulators,” *Phys. Rev. Lett.* **106**, 136802 (2011).
- [28] Suk Bum Chung and Shou-Cheng Zhang, “Detecting the majorana fermion surface state of  $^3\text{He-B}$  through spin relaxation,” *Phys. Rev. Lett.* **103**, 235301 (2009).
- [29] Luka Trifunovic and Piet W. Brouwer, “Higher-order bulk-boundary correspondence for topological crystalline phases,” *Phys. Rev. X* **9**, 011012 (2019).
- [30] Shinsei Ryu, Andreas P. Schnyder, Akira Furusaki, and Andreas W. W. Ludwig, “Topological insulators and superconductors: tenfold way and dimensional hierarchy,” *New Journal of Physics* **12**, 065010 (2010).
- [31] Ching-Kai Chiu, Jeffrey C. Y. Teo, Andreas P. Schnyder, and Shinsei Ryu, “Classification of topological quantum matter with symmetries,” *Rev. Mod. Phys.* **88**, 035005 (2016).
- [32] Robert M Wald, *General relativity* (Chicago Univ. Press, Chicago, IL, 1984).
- [33] Mikio Nakahara, *Geometry, topology and physics*, Graduate student series in physics (Hilger, Bristol, 1990).
- [34] The relation between two coordinates  $\{e_\mu\}$  and  $\{e_i\}$  is completely specified by the tetrad  $e^i{}_\mu \equiv \partial x^i / \partial x^\mu$ . Then,  $g_{\mu\nu} = \eta_{ij} e^i{}_\mu e^j{}_\nu$ ,  $\gamma^\mu = \gamma^i e_i{}^\mu$ . The spin connection takes the form as  $\Gamma_\mu = \frac{i}{2} \Gamma_\mu{}^{ij} \Sigma_{ij}$  with  $\Sigma_{ij} = \frac{i}{2} [\gamma_i, \gamma_j]$  and  $\Gamma_\mu{}^{ij} = e^i{}_\nu \nabla_\mu e^{j\nu}$ .
- [35] José González, Francisco Guinea, and M. Angeles H. Vozmediano, “Continuum approximation to fullerene molecules,” *Phys. Rev. Lett.* **69**, 172–175 (1992).
- [36] A. A. Abrikosov, Jr, “Dirac operator on the Riemann sphere,” *ArXiv High Energy Physics - Theory e-prints* (2002), [hep-th/0212134](https://arxiv.org/abs/hep-th/0212134).
- [37] V. Parente, P. Lucignano, P. Vitale, A. Tagliacozzo, and F. Guinea, “Spin connection and boundary states in a topological insulator,” *Phys. Rev. B* **83**, 075424 (2011).
- [38] Yi Zhang and Ashvin Vishwanath, “Anomalous aharonov-bohm conductance oscillations from topological insulator surface states,” *Phys. Rev. Lett.* **105**, 206601 (2010).
- [39] Ken-Ichiro Imura, Yukinori Yoshimura, Yositake Takane, and Takahiro Fukui, “Spherical topological insulator,” *Phys. Rev. B* **86**, 235119 (2012).
- [40] Yositake Takane and Ken-Ichiro Imura, “Unified description of dirac electrons on a curved surface of topological insulators,” *Journal of the Physical Society of Japan* **82**, 074712 (2013), <https://doi.org/10.7566/JPSJ.82.074712>.
- [41] J I Kapusta and P V Landshoff, “Finite-temperature field theory,” *Journal of Physics G: Nuclear and Particle Physics* **15**, 267 (1989).
- [42] Ting-Pong Choy, K. T. Law, and Tai-Kai Ng, “Magnetic impurities on the surface of topological superconductor,” (2013), [arXiv:1301.2068](https://arxiv.org/abs/1301.2068) [cond-mat.supr-con].
- [43] Chang-An Li, Song-Bo Zhang, Jian Li, and Björn Trauzettel, “Higher-order fabry-pérot interferometer from topological hinge states,” *Phys. Rev. Lett.* **127**, 026803 (2021).
- [44] Adam Yanis Chaou, Piet W. Brouwer, and Nicholas Sedlmayr, “Hinge states of second-order topological insulators as a mach-zehnder interferometer,” *Phys. Rev. B* **107**, 035430 (2023).